ACS Photonics

Article

pubs.acs.org/journal/apchd5

Strong Magnetic Response of Optical Nanofibers

Shaghik Atakaramians,*[,†] Andrey E. Miroshnichenko,[‡] Ilya V. Shadrivov,[‡] Ali Mirzaei,[‡] Tanya M. Monro,[§] Yuri S. Kivshar,[‡] and Shahraam Afshar V.[§]

[†]Institute of Photonics and Optical Science, School of Physics, The University of Sydney, Sydney NSW 2006, Australia

[‡]Nonlinear Physics Centre, Research School of Physics and Engineering, Australian National University, Canberra ACT 2601, Australia

[§]Laser Physics and Photonic Devices Laboratories, School of Engineering, University of South Australia, Mawson Lakes SA 5095, Australia

Institute for Photonics and Advanced Sensing, The University of Adelaide, Adelaide SA 5005, Australia

S *Supporting Information*

ABSTRACT: We introduce a new platform to achieve a strong magnetic response in optical fibers with nanoscale dimension. We reveal that for a coupled dipole−fiber system an electric dipole placed near an optical nanofiber can produce strong magnetic response. We show that the magnetic and electric response of such a system depends on the orientation of the dipole source with respect to the fiber. Using the multipole expansion method, we demonstrate that it is possible to suppress the electric response and preferentially enhance the magnetic resonance of a coupled dipole−fiber system, in such a way that the energy in the magnetic mode can be made 2 orders of magnitude higher than that of the electric mode of the system. This nanophotonic system opens up new possibilities to develop low-dimensional nanodevices with enhanced magnetic response.

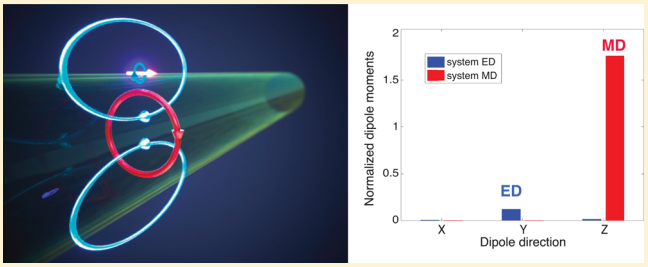

KEYWORDS: *optical fibers, nanophotonics, optical magnetism, multipole decomposition, coupled dipole−fiber system*

The magnetic response of most natural materials is usually weak due to the negligible contribution of electronic spin at high frequencies, which leads to small induced magnetic dipoles.[1] As a result, the permeability of most natural materials in optics is assumed to be equal to the permeability in a vacuum. For a stronger magnetic response, one can excite electric currents in artificial metallic loops, which allow access to a wide range of effective values of μ, including negative values. These loop currents are the building blocks of metallic metamaterials, which have been used to design structures with negative refractive index[2−5] for applications such as cloaking[6] and superlensing.[7] The main drawback with these metamaterial structures is the high Ohmic loss of metallic parts at optical frequencies. Recently, it has been shown that dielectric nanoparticles with a high refractive index can also lead to a strong magnetic response.[8−20] The Mie scattering of light from high-index dielectric nanoparticles shows a series of alternative magnetic and electric dipole and multipole resonances vs frequency associated with induced magnetic and electric resonant modes. This has been studied for particles of different sizes and shapes including spheres, rods, and disks.[8,9,12,18,20−24]

Seemingly in a different field of research, the interaction between quantum emitters and electromagnetic modes of a cavity, recognized as cavity quantum electrodynamics (CQED),[25,26] has been explored for both weak and strong coupling regimes in different cavity structures,[27] such as microspheres,[28−30] microtoroids,[31,32] microdisks,[33] and Fabry−Perot microresonators.[34] The modification of quantum emitters' properties, such as radiation power and decay rate, by coupling with dielectric waveguides has also been studied.[35−43] The radiation peaks of coupled quantum emitters with optical fibers have been studied theoretically, observed experimentally,[35,44] and associated with the whispering gallery modes (WGMs) of fibers.[40,42,43] Coupling of a quantum emitter into guided and radiation modes of an optical fiber has been studied,[35,38,40−42,45−50] being identified as a potential platform for developing devices for quantum information technology.[46,49,50] However, until now the research of such systems has been focused on the study of higher order radiation modes associated with high-Q cavity resonances.

In this paper, we suggest a new platform to achieve a strong magnetic response, based on a localized source on the surface of a nanofiber, hence establishing a connection between dielectric metamaterials based on Mie scattering and dipole−cavity interaction. We demonstrate that the first radiation peak of a localized source (electric dipole) in the vicinity of a relatively low-index optical waveguide can have *a strong induced magnetic response*. We demonstrate that such a structure has

Received: January 20, 2016
Published: May 13, 2016

DOI: 10.1021/acsphotonics.6b00030
ACS Photonics 2016, 3, 972−978

radiation peaks wherein the contribution of TE and TM harmonics depends on the orientation of the source with respect to the fiber axis. By decomposing the scattered electric field into the excited harmonics, we find that the first radiation peak of the system is induced by strong electric or magnetic dipole response. We show that the dipole−fiber system can suppress the electric dipole response and preferentially enhance the magnetic resonance. Unlike high-index refractive nanoparticles, here we report the existence of a strong magnetic response with a moderate refractive index, which suggests developing of novel nanophotonic devices based on optical-fiber technologies,[51] with tunable magnetic and electric responses.

RESULTS AND DISCUSSION

We study a system that consists of an electric dipole excited at a fixed frequency (below we consider the wavelength λ = 700 nm) placed at the core-clad interface (on the x-axis) of an air-clad nanofiber, with telluride as the hosting material. Tellurite is a soft glass with a refractive index n = 2.025. The main results presented here are true for any choice of moderate and high refractive index, where there is a distinct first radiation peak. It is shown that higher core-clad refractive index contrast leads to enhanced emission of a dipole at the vicinity of an optical fiber.[43] Incorporating single emitters within tellurite step-index fibers has recently been reported as a platform for hybrid quantum-photonics devices.[48] We assume that the fiber is oriented along the z-axis and the center of the coordinates is at the center of the fiber cross section as shown in Figure 1. Such

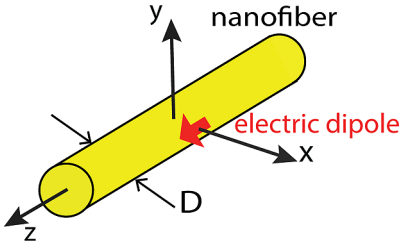

Figure 1. Schematic of coupled dipole−fiber system.

a system has strong radiation peaks associated with the WGMs formed in the cross section of the nanofiber.[43] The total emitted power by the system can be expressed as the summation of the powers of radiated and guided modes:[49,52]

$$P_{\text{total}} = \sum_j P_j + \sum_\nu \int_0^{Q_{\max}} P_\nu(Q)\, \mathrm{d}Q \tag{1}$$

where $Q = (D/2)(k^2 - \beta^2)^{1/2}$, D is the core diameter, $k = 2\pi/\lambda$, β is the propagation constant, and $Q_{\max} = kD/2$. The $P_j = |a_j|^2 N_j$ and $P_\nu = |a_\nu|^2 N_\nu$ are respectively the power captured in the guided mode j and the radiation mode ν of the fiber, j and ν are the azimuthal mode indices, and $N_{j,\nu} = (1/2)\int_{A_\infty}(\mathbf{e}_{j,\nu} \times \mathbf{h}^*_{j,\nu})\cdot \hat{z}\,dA$ is a normalization term. The coupling coefficients a_j and a_ν are given by

$$|a_{j,\nu}|^2 = \frac{\omega^2}{16 N_{j,\nu}^2} |\mathbf{e}^*_{j,\nu}(\mathbf{r}_0)\cdot \mathbf{p}_0(\mathbf{r}_0)|^2 \tag{2}$$

Here, $\mathbf{e}_{j,\nu}$ and $\mathbf{h}_{j,\nu}$ are jth (νth) guided electric and magnetic fields of the fiber, respectively, and $\mathbf{p}_0(\mathbf{r}_0)$ is the dipole vector at the position of $\mathbf{r}_0$. Equation 2 describes the dipole−electromagnetic field interaction. The integration in eq 1 for the radiated power is due to the continuous nature of the allowed propagation constant value, redefined in terms of Q.[48] The radiation modes are formed by a superposition of TE- and TM-like elementary modes of the fiber with relatively small longitudinal electric and magnetic fields, respectively.[49,52]

The normalized radiated power and the contribution of both TE and TM components corresponding to the z- and r-oriented dipole excitations are shown in Figure 2a and c. The total radiated power is normalized to the total radiated dipole power from the telluride glass. When the electric dipole source is oriented along the z-direction, the total radiation has a dominant TM component, which defines the position of the resonance peaks (see Figure 2a). This can be explained in terms of the excitation fields: a z-oriented dipole couples strongly into a mode with a large z-component electric field (see eq 2); thus it can mainly couple into TM radiated modes of the fiber. The position of these peaks overlaps with the position of the TE whispering gallery mode (TE-WGM) resonances (blue triangles in Figure 2a) of a two-dimensional (2D) microdisk calculated independently by solving Maxwell's equations for a 2D circular disk with a diameter equal to that of the fiber.[43]

The radiated power of the r-oriented dipole is shown in Figure 2c. The four first radiation peaks have both TE and TM radiation contributions, while higher order radiation peaks have only a strong TE contribution; that is, the position of higher order peaks is defined by the position of TE radiation mode peaks of the fiber. This can be explained in terms of the excitation fields: an r-oriented dipole couples strongly into the modes with a large r-component electric field (see eq 2); in this case these modes are the TM radiation modes of fiber and the TM whispering gallery mode (TM-WGM) resonances. As a result of TM-WGM excitation, the TE radiation modes of fiber are also excited. Thus, the first four radiation peaks do not align with the positions of WGM resonances due to the existence of both polarizations, while higher order radiation peaks overlap with the position of the TM-WGM resonances (red triangles in Figure 2c) of a two-dimensional microdisk calculated independently.

We employ the electromagnetic multipole expansion to decompose the fields radiated by the system in terms of electric and magnetic multipoles, which represent the spatially localized sources, i.e., electric charges and currents.[53,54] We use the commercially available numerical software CST Microwave Studio to calculate the electric field of the system ($\mathbf{E}_{\text{total}}$) and the localized source ($\mathbf{E}_{\text{source}}$) at the position of the first radiation peak. The center of the coordinates is located at the center of the fiber cross section. The fiber is oriented along the z-axis, and a discrete current port is defined to represent an electric dipole on the x-axis ($x = D/2$). We first use "open" boundary conditions (a perfectly matched layer with minimum reflection) in the z-direction and "open (add space)" boundary conditions (similar to open with an extra space) in both the x- and y-directions, to represent an infinitely long fiber along the z-axis in free space. Then we change the boundary condition along the z-direction to "open (add space)". This is equivalent to a finite fiber (nanorod); in this case L = 4 μm long ($L/\lambda > 5.7$). The near-field and far-field results are found to be similar in both cases, indicating that the chosen length for the fiber is long enough to represent an infinite fiber. The limited length of the fiber is required for the far-field decomposition discussed below.

DOI: 10.1021/acsphotonics.6b00030
ACS Photonics 2016, 3, 972−978

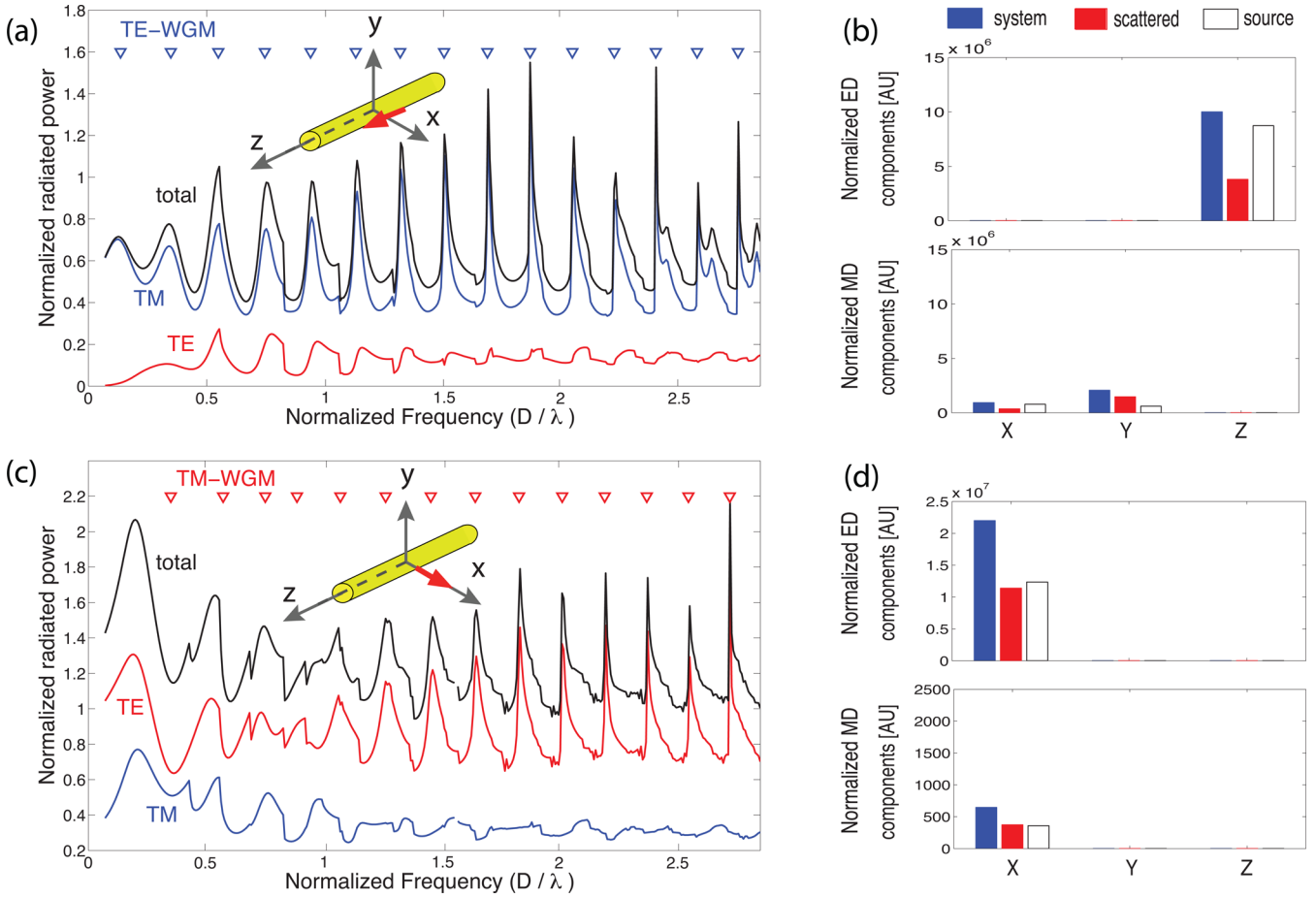

Figure 2. Normalized radiated power (total, TE and TM) of a dipole−fiber system with (a) *z*- and (c) *r*-oriented excitation. All the radiated powers are normalized to the dipole radiation power in bulk tellurite glass. The radius of the (*m*, 0) resonances of 2D TE- and TM-WGMs is shown respectively with blue and red triangles. The normalized Cartesian ED and MD moments of the system at the position of the first radiation peak: (b) *z*- and (d) *r*-oriented dipole excitation. The normalized frequencies (diameters) are 0.128 and 0.2, respectively.

In general, the scattered electric field of a system, which is excited by a monochromatic plane wave, with the electric field amplitude E_0, angular frequency ω, and wave vector $\mathbf{k}$, can be written in spherical coordinates in the form of the following multipole expansion:[54]

$$\mathbf{E}_s(r, \theta, \phi) = E_0 \sum_{l=1}^{\infty} \sum_{m=-1}^{l} i^l [\pi(2l+1)]^{1/2} \times \left\{ \frac{1}{k} a_E(l, m) \nabla \times h_l^{(1)}(kr)\, \mathbf{X}_{lm}(\theta, \phi) + a_M(l, m)\, h_l^{(1)}(kr)\, \mathbf{X}_{lm}(\theta, \phi) \right\} \quad (3)$$

where $\mathbf{X}_{lm}$ and $h_l^{(1)}$ are the normalized vector spherical harmonics and the spherical Hankel functions of the first kind, respectively. The coefficients $a_E(l, m)$ and $a_M(l, m)$ represent the amplitudes of electric and magnetic (l, m) multipoles. These coefficients can be calculated once the scattered electric field $\mathbf{E}_s$ is known, by using the orthogonality of the spherical harmonics (see eqs S1 and S2 in the Supporting Information).[54] Consequently, the Cartesian multipole moments can be calculated from the coefficients $a_E(l, m)$ and $a_M(l, m)$ (see eqs S3 and S4 in the Supporting Information).[54] In general, the multipole decomposition depends on the origin of the coordinate system. Here, the origin is chosen to be at the center of the cross section of the fiber. Equation 3 can also be employed to decompose the total electric field of the coupled dipole−fiber system. Here, the system is excited using a dipole source; therefore for decompostion of the fields we normalize the electric fields to E_0 by assuming $E_0 = 1$.

We have calculated the noramlized Cartesian electric and magnetic dipole moments (ED and MD, respectively) of a *z*-oriented dipole on the surface of the fiber using eqs S3 and S4, at the position of the first radiation peak (normalized frequency/diameter 0.128), as shown in Figure 2b. The ED and MD moments are normalized to C_p and C_m, respectively (see eqs S3 and S4 in the Supporting Information). Unsurprisingly an off-axis *z*-oriented dipole by itself (source) has a strong *z*-oriented ED moment, relatively weak MD moments, and higher order electric quadrupole components (see Figure S1a in the Supporting Information).[53] We observe that the inclusion of the nanofiber enhances the ED and MD components of the system with ED remaining the dominant component.

Figure 2d shows the noramlized Cartesian ED and MD moments by an *r*-oriented electric dipole located on the *x*-axis (off-centered *x*-oriented). The dipole components confirm a strong ED moment along the *x*-direction and negligible MD moment for source only. By the presence of the fiber, the ED component at the position of the first peak (normalized

DOI: 10.1021/acsphotonics.6b00030
ACS Photonics 2016, 3, 972−978

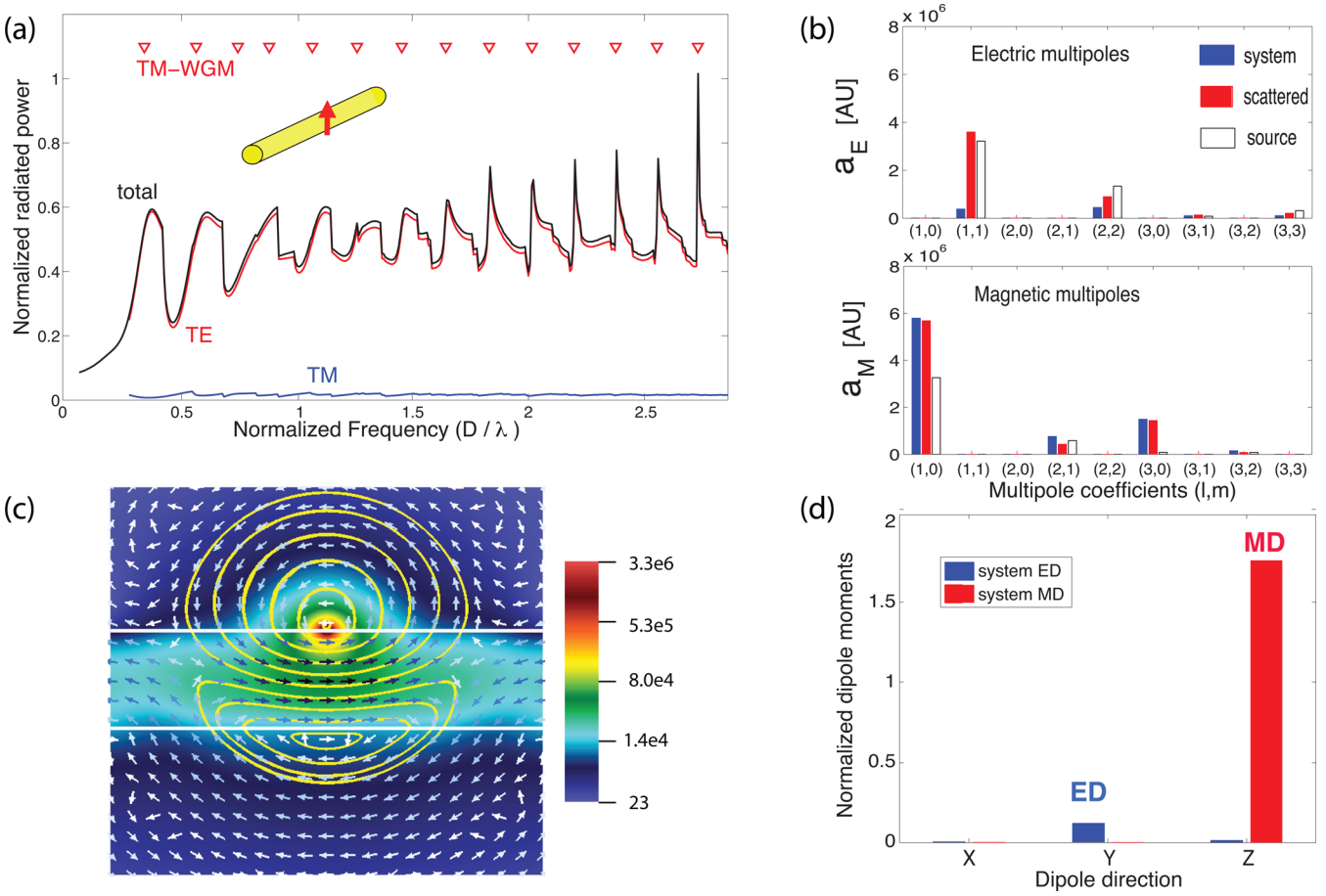

Figure 3. Magnetic response of a nanofiber: (a) Normalized radiated power for a system with a ϕ-oriented excitation. The radius of the (m, 0) resonances of 2D TM-WGMs are shown in red triangles. (b) Electric and magnetic multipole coefficients of the total electric field of the system (blue bars) and the source (white bars). (c) Magnetic field in the xz-plane, where white horizontal lines represent the core-clad interface of the fiber. (d) Normalized ED and MD moments of the system at the position of the first radiation peak. The dipole moments are normalized to dipole moments of the system without the fiber (source only).

frequency/diameter 0.2) is further enhanced (remaining the dominant component), and higher order electric components also start appearing (see Figure S1b in the Supporting Information). The emergence of quadrupoles in the system also explains the offset between the radiation peaks and the position of the WGM resonances observed in Figure 2c.

The normalized power radiated by a ϕ-oriented dipole−fiber system is shown in Figure 3a. The total radiated power has a TE dominant component, which defines the position of the peaks. In terms of dipole excitation, a ϕ-oriented dipole couples strongly to a mode with a large ϕ-component electric field (see eq 2); thus it mainly couples into TE-like radiated modes. This also explains the alignment of the radiation peaks with the position of the TM-WGM resonances (shown with red triangles in Figure 3a) for the 2D microdisk. Figure 3b shows the decomposition results (spherical electric and magnetic multipoles) at the position of the first peak (normalized frequency/diameter 0.386). Only positive m multipole components are shown, due to the symmetry of $a_{E,M}(l, m)$ and $a_{E,M}(l, -m)$ components. The source is located on the x-axis and core-clad interface, which represents an off-centered y-oriented dipole, i.e., strong $a_E(1, \pm 1)$ components (Figure 3b) leading to a strong P_y (see Figure S2a in the Supporting Information). In the presence of a fiber, the contribution of $a_E(1, 1)$ is suppressed, while the $a_M(1, 0)$ component is enhanced so that $a_M(1, 0)/a_E(1, 1) \approx 15$. The $a_E(1, 1)$ component of the scattered field is comparable only to that of the source, showing that the nanofiber generates a strong $a_E(1, 1)$ component that counteracts that of the source, thus suppressing the electric dipole moment of the coupled dipole−fiber system.

Figure 3c shows the magnetic field of the system in the xz-plane. The white horizontal lines represent the core-clad interface of the fiber. The arrows and contour lines represent the direction and field lines of the magnetic field, respectively. The figure demonstrates a magnetic field along the z-direction in the fiber. Moreover, the magnetic field outside the fiber is in the opposite direction with respect to that inside the fiber. This indicates and confirms the formation of a magnetic dipole (along the z-axis) in the system. To quantify the dipole moments, we normalize the dipole moments of the system to that of the source (see Figure 3d). Blue and red colors represent the normalized ED and MD moments, respectively. The ED component is suppressed dramatically (~0.12), while the MD component is enhanced (~1.8 times), leading to an overall strong magnetic response. The results in Figure 3d are proportional to the effective electric and magnetic polarizability, indicating that the effective magnetic polarizability is more than 1 order of magnitude (~15 times) higher than the effective electric polarizability in the system.

DOI: 10.1021/acsphotonics.6b00030
ACS Photonics 2016, 3, 972−978

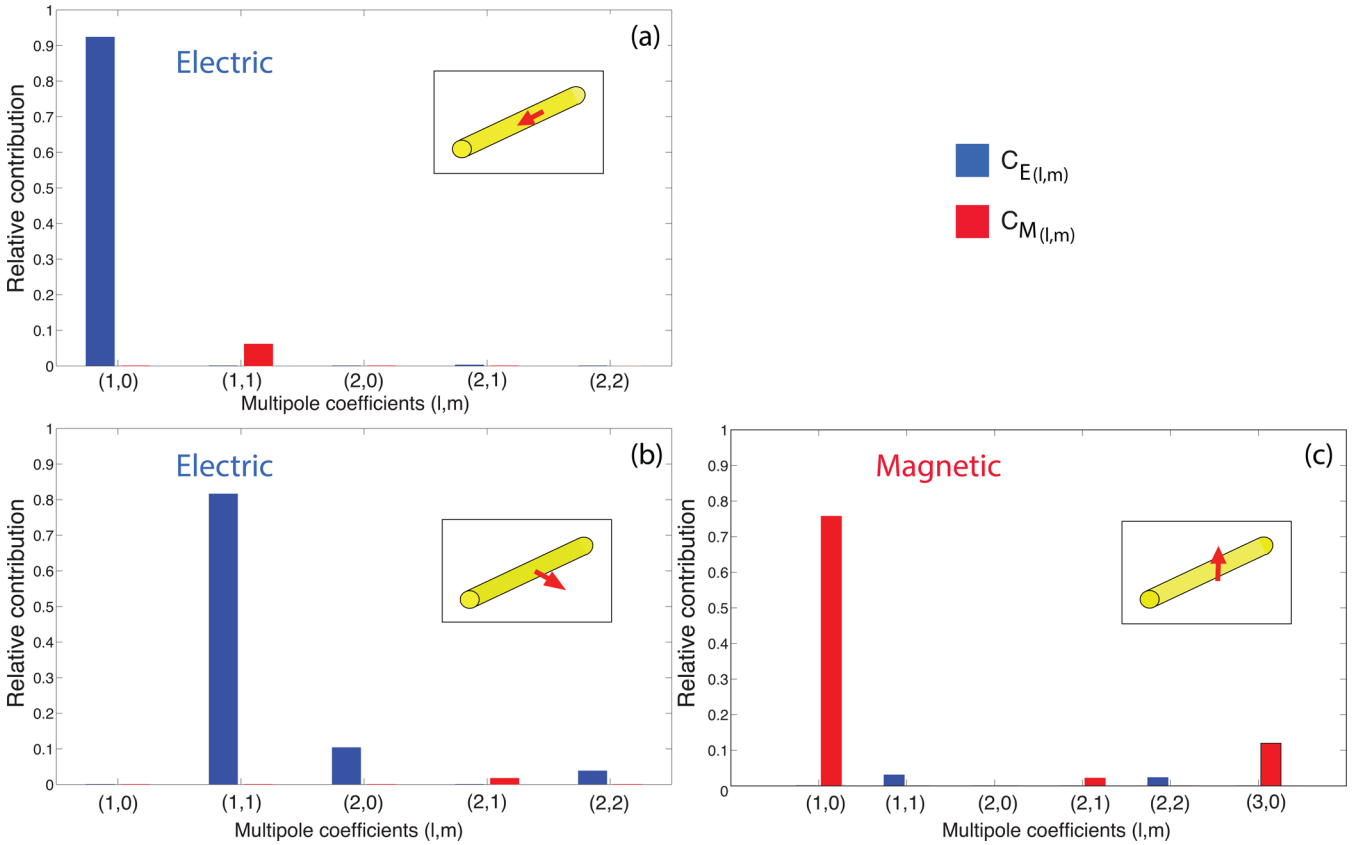

Figure 4. Relative contribution of multipole coefficients (l, m) in the total enegry of the system when the excitation is a (a) z-, (b) r-, and (c) ϕ-oriented electric dipole. The inset shows the system configuration for each case.

Having multipole coefficients, the scattering cross section, which defines the fraction of incident energy coupled into the scattered field, can be derived as[54]

$$\mathbf{C}_s = \frac{\pi}{k^2}\sum_{l=1}^{\infty}\sum_{m=-1}^{l}(2l+1)[|a_E(l,m)|^2 + |a_M(l,m)|^2] \tag{4}$$

The terms of the series determine the contribution of each multipole excitation to the overall scattering cross section. For a plane wave excitation, eq 4 is normalized to the total energy in the plane wave (see eqs S1 and S2 in the Supporting Information). For the dipole excitation we assumed $E_0 = 1$; thus we nomalize the contribution of each electric and magnetic multipole to the total radiant energy in the system calculated from the numerical simulation (W_s). Therefore, the relative contribution of each multipole component is defined as $C_{E,M}(l, m) = \pi(2l+1)|a_{E,M}(l,m)|^2/(k^2W_s)$. This also defines the energy distribution in the system in terms of spatially localized sources.

Figure 4 shows the relative contribution of each multipole in the total energy of the coupled dipole−fiber system. The horizontal axis shows the multipole scattering coefficients (l, m). Due to symmetry of $C_{E,M}(l, m)$ and $C_{E,M}(l, -m)$ components (inherited from $a_{E,M}(l, \pm m)$, respectively), the total contribution of both components is presented at (l, m). With a z-oriented dipole excitation (Figure 4a) the energy couples predominantly (>90%) in the $C_E(1, 0)$ component; that is, the system represents an enhanced electric dipole along the z-axis. With the presence of an r-oriented dipole (Figure 4b), most of the energy also couples into electric mulitpoles with a strong contribution from $C_E(1, 1)$, representing an electric dipole along the x-axis. The presence of quadrupoles [$C_E(2, 0)$ and $C_E(2, 2)$] in the system also explains the offset between the radiation peaks and the position of the WGMs observed in Figure 2c. This is while a system with ϕ-oriented dipole excitation (Figure 4c) behaves in a completely different way. There exist a strong contribution (more than 75%) from $C_M(1, 0)$ (z-oriented magnetic dipole) and a small but considerable contribution (more than 10%) from octupole magnetic component $C_M(3,0)$ in the total energy distribution of the system, while the contribution of the source is dramatically suppressed so that $C_M(1, 0)/2C_E(1, 1) \approx 112$ (the factor 2 is to consider the symmetry of $C_E(1, 1)$ and $C_E(1, -1)$).

CONCLUSION AND DISCUSSION

We have introduced a new platform that allows accessing a strong magnetic response in optical fibers with nanoscale dimensions (nanofiber). The electric response of a system of an electric dipole, and a nanofiber can be suppressed preferentially while its magnetic response is enhanced by more than 2 orders of magnitude. This strong magnetic response is observed in a system with a relatively moderate refractive index. We believe these results will pave the way to developing novel nanofiber devices with a large induced magnetic response.

The concept developed here can be applied to any part of the electromagnetic spectrum depending on the application. For example, a free-standing subwavelength fiber with the diameter on the order of a few millimeters or a few hundred micrometers can be used to demonstrate the concept in the microwave or terahertz regime, respectively. In the optical frequency domain, the concept can be demonstrated in fibers with relatively

DOI: 10.1021/acsphotonics.6b00030
ACS Photonics 2016, 3, 972−978

moderate index glasses such as tellurite with diameters on the order of a few hundred nanometers. Both free-standing tellurite optical nanowires with a 100 nm diameter[55] and tellurite microstructured tapered optical fibers with core diameters of 320−80 nm[56] have been reported and can be exploited for the concept reported here.

■ ASSOCIATED CONTENT

Supporting Information

The Supporting Information is available free of charge on the ACS Publications website at DOI: 10.1021/acsphotonics.6b00030.

Derivation of multipole coefficients in spherical and Cartesian coordinates and far-field power patterns from numerical simulation (PDF)

■ AUTHOR INFORMATION

Corresponding Author

*E-mail (S. Atakaramians): shaghik.a@sydney.edu.au.

Notes

The authors declare no competing financial interest.

■ ACKNOWLEDGMENTS

S.A. acknowledges support from the Australian Research Council (ARC) (DE140100614). T.M.M. acknowledges the support of an ARC Georgina Sweet Laureate Fellowship. Y.S.K. thanks S. Turitsyn and M. Sumetsky of the Aston University for useful discussion of the physics of nanowires and also acknowledges a visiting fellowship from the Liverhulme Trust.

■ REFERENCES

(1) Krasnok, A.; Makarov, S.; Petrov, M.; Savelev, R.; Belov, P.; Kivshar, Y. Towards all-dielectric metamaterials and nanophotonics. *Proc. SPIE* **2015**, *9502*, 950203.

(2) Shalaev, V. M. Optical negative-index metamaterials. *Nat. Photonics* **2007**, *1*, 41−48.

(3) Zheludev, N. I. The Road Ahead for Metamaterials. *Science* **2010**, *328*, 582−583.

(4) Soukoulis, C. M.; Wegener, M. Optical Metamaterials-More Bulky and Less Lossy. *Science* **2010**, *330*, 1633−1634.

(5) Zheludev, N. I.; Kivshar, Y. S. From metamaterials to metadevices. *Nat. Mater.* **2012**, *11*, 917−924.

(6) Leonhardt, U. Optical Conformal Mapping. *Science* **2006**, *312*, 1777−1780.

(7) Pendry, J. B. Negative Refraction Makes a Perfect Lens. *Phys. Rev. Lett.* **2000**, *85*, 3966−3969.

(8) Peng, L.; Ran, L.; Chen, H.; Zhang, H.; Kong, J. A.; Grzegorczyk, T. M. Experimental Observation of Left-Handed Behavior in an Array of Standard Dielectric Resonators. *Phys. Rev. Lett.* **2007**, *98*, 157403.

(9) Schuller, J. A.; Zia, R.; Taubner, T.; Brongersma, M. L. Dielectric Metamaterials Based on Electric and Magnetic Resonances of Silicon Carbide Particles. *Phys. Rev. Lett.* **2007**, *99*, 107401.

(10) Zhao, Q.; Du, B.; Kang, L.; Zhao, H.; Xie, Q.; Li, B.; Zhang, X.; Zhou, J.; Li, L.; Meng, Y. Tunable negative permeability in an isotropic dielectric composite. *Appl. Phys. Lett.* **2008**, *92*, 051106.

(11) Popa, B. I.; Cummer, S. A. Compact Dielectric Particles as a Building Block for Low-Loss Magnetic Metamaterials. *Phys. Rev. Lett.* **2008**, *100*, 207401.

(12) Vynck, K.; Felbacq, D.; Centeno, E.; Cabuz, A. I.; Cassagne, D.; Guizal, B. All-Dielectric Rod-Type Metamaterials at Optical Frequencies. *Phys. Rev. Lett.* **2009**, *102*, 133901.

(13) Zhao, Q.; Zhou, J.; Zhang, F.; Lippens, D. Mie resonance-based dielectric metamaterials. *Mater. Today* **2009**, *12*, 60−69.

(14) Evlyukhin, A. B.; Reinhardt, C.; Seidel, A.; Lukyanchuk, B. S.; Chichkov, B. N. Optical response features of Si-nanoparticle arrays. *Phys. Rev. B: Condens. Matter Mater. Phys.* **2010**, *82*, 045404.

(15) Ginn, J. C.; Brener, I.; Peters, D. W.; Wendt, J. R.; Stevens, J. O.; Hines, P. F.; Basilio, L. I.; Warne, L. K.; Ihlefeld, J. F.; Clem, P. G.; Sinclair, M. B. Realizing Optical Magnetism from Dielectric Metamaterials. *Phys. Rev. Lett.* **2012**, *108*, 097402.

(16) Kuznetsov, A. I.; Miroshnichenko, A. E.; Fu, Y. H.; Zhang, J.; Lukyanchuk, B. Magnetic light. *Sci. Rep.* **2012**, *2*, 492.

(17) Fu, Y. H.; Kuznetsov, A. I.; Miroshnichenko, A. E.; Yu, Y. F.; Lukyanchuk, B. Directional visible light scattering by silicon nanoparticles. *Nat. Commun.* **2013**, *4*, 1527.

(18) Staude, I.; Miroshnichenko, A.; Decker, M.; Fofang, N.; Liu, S.; Gonzales, E.; Dominguez, J.; Luk, T.; Neshev, D.; Brener, I.; Kivshar, Y. Tailoring directional scattering through magnetic and electric resonances in subwavelength silicon nanodisks. *ACS Nano* **2013**, *7*, 7824−7832.

(19) Bi, K.; Guo, Y.; Liu, X.; Zhao, Q.; Xiao, J.; Lei, M.; Zhou, J. Magnetically tunable Mie resonance-based dielectric metamaterials. *Sci. Rep.* **2014**, *4*, 7001.

(20) Habteyes, T.; Staude, I.; Chong, K.; Dominguez, J.; Decker, M.; Miroshnichenko, A.; Kivshar, Y.; Brener, I. Near-Field Mapping of Optical Modes on All-Dielectric Silicon Nanodisks. *ACS Photonics* **2014**, *1*, 794−798.

(21) Cao, L.; Fan, P.; Barnard, E. S.; Brown, A. M.; Brongersma, M. L. Tuning the Color of Silicon Nanostructures. *Nano Lett.* **2010**, *10*, 2649−2654.

(22) Cao, L.; Fan, P.; Barnard, E. S.; Brown, A. M.; Brongersma, M. L. Tuning the Color of Silicon Nanostructures. *Nano Lett.* **2010**, *10*, 2649−2654.

(23) Evlyukhin, A.; Eriksen, R.; Cheng, W.; Beermann, J.; Reinhardt, C.; Petrov, A.; Prorok, S.; Eich, M.; Chichkov, B.; Bozhevolnyi, S. Optical spectroscopy of single Si nanocylinders with magnetic and electric resonances. *Sci. Rep.* **2014**, *4*, 4126.

(24) Brongersma, M. L.; Cui, Y.; Fan, S. Light management for photovoltaics using high-index nanostructures. *Nat. Mater.* **2014**, *13*, 451−460.

(25) Purcell, E. M. Spontaneous emission probabilities at radio frequencies. *Phys. Rev.* **1946**, *69*, 681.

(26) Berman, P. *Cavity Quantum Electrodynamics*, 1st ed.; Academic Press, 1993.

(27) Vahala, K. J. Optical microcavities. *Nature* **2003**, *424*, 839−846.

(28) Vernooy, D.; Furusawa, A.; Georgiades, N.; Ilchenko, V.; Kimble, H. Cavity QED with high-(Q) whispering gallery modes. *Phys. Rev. A: At., Mol., Opt. Phys.* **1998**, *57*, 2293−2296.

(29) Schniepp, H.; Sandoghdar, V. Spontaneous Emission of Europium Ions Embedded in Dielectric Nanospheres. *Phys. Rev. Lett.* **2002**, *89*, 257403.

(30) Spillane, S.; Kippenberg, T.; Painter, O.; Vahala, K. Ideality in a Fiber-Taper-Coupled Microresonator System for Application to Cavity Quantum Electrodynamics. *Phys. Rev. Lett.* **2003**, *91*, 2−5.

(31) Armani, D. K.; Kippenberg, T. J.; Spillane, S. M.; Vahala, K. J. Ultra-high-Q toroid micro cavity on an chip. *Nature* **2003**, *421*, 925−928.

(32) Aoki, T.; Dayan, B.; Wilcut, E.; Bowen, W. P.; Parkins, A. S.; Kippenberg, T. J.; Vahala, K. J.; Kimble, H. J. Observation of strong coupling between one atom and a monolithic microresonator. *Nature* **2006**, *443*, 671−674.

(33) Kiraz, A.; Michler, P.; Becher, C.; Gayral, B.; Imamofülu, A.; Zhang, L.; Hu, E.; Schoenfeld, W. V.; Petroff, P. M. Cavity-quantum electrodynamics using a single InAs quantum dot in a microdisk structure. *Appl. Phys. Lett.* **2001**, *78*, 3932−3934.

(34) Schmidt, M. A.; Lei, D. Y.; Wondraczek, L.; Nazabal, V.; Maier, S. A. Hybrid nanoparticle-microcavity-based plasmonic nanosensors with improved detection resolution and extended remote-sensing ability. *Nat. Commun.* **2012**, *3*, 1108.

(35) Owen, J. F.; Barber, P. W.; Dorain, P. B.; Chang, R. K. Enhancement of Fluorescence Induced by Microstructure Resonances of a Dielectric Fiber. *Phys. Rev. Lett.* **1981**, *47*, 1075−1078.

DOI: 10.1021/acsphotonics.6b00030
ACS Photonics 2016, 3, 972−978

(36) Heinzen, D. L.; Feld, M. S. Vacuum Radiative Level Shift and Spontaneous-Emission Linewidth of an Atom in an Optical Resonator. *Phys. Rev. Lett.* **1987**, *59*, 2623−2626.
(37) Björk, G.; Machida, S.; Yamamoto, Y.; Igeta, K. Modification of spontaneous emission rate in planar dielectric microcavity structures. *Phys. Rev. A: At., Mol., Opt. Phys.* **1991**, *44*, 669−681.
(38) Chu, D. Y.; Ho, S.-T. Spontaneous emission from excitons in cylindrical dielectric waveguides and the spontaneous-emission factor of microcavity ring lasers. *J. Opt. Soc. Am. B* **1993**, *10*, 381−390.
(39) Janowicz, M.; Zakowicz, W. Quantum radiation of a harmonic oscillator near the planar dielectric-vacuum interface. *Phys. Rev. A: At., Mol., Opt. Phys.* **1994**, *50*, 4350−4364.
(40) Zakowicz, W.; Janowicz, M. Spontaneous emission in the presence of a dielectric cylinder. *Phys. Rev. A: At., Mol., Opt. Phys.* **2000**, *62*, 013820.
(41) Klimov, V. V.; Ducloy, M. Spontaneous emission rate of an excited atom placed near a nanofiber. *Phys. Rev. A: At., Mol., Opt. Phys.* **2004**, *69*, 013812.
(42) Fussell, D. P.; McPhedran, R.; de Sterke, C. M. Decay rate and level shift in a circular dielectric waveguide. *Phys. Rev. A: At., Mol., Opt. Phys.* **2005**, *71*, 013815.
(43) Afshar V, S.; Henderson, M. R.; Greentree, A. D.; Gibson, B. C.; Monro, T. M. Self-formed cavity quantum electrodynamics in coupled dipole cylindrical-waveguide systems. *Opt. Express* **2014**, *22*, 11301−11311.
(44) Wang, P.; Wang, Y.; Yang, Z.; Guo, X.; Lin, X.; Yu, X.-C.; Xiao, Y.-F.; Fang, W.; Zhang, L.; Lu, G.; Gong, Q.; Tong, L. Single-Band 2-nm-Line-Width Plasmon Resonance in a Strongly Coupled Au Nanorod. *Nano Lett.* **2015**, *15*, 7581.
(45) Le Kien, F.; Dutta Gupta, S.; Balykin, V. I.; Hakuta, K. Spontaneous emission of a cesium atom near a nanofiber: Efficient coupling of light to guided modes. *Phys. Rev. A: At., Mol., Opt. Phys.* **2005**, *72*, 032509.
(46) Le Kien, F.; Hakuta, K. Cavity-enhanced channeling of emission from an atom into a nanofiber. *Phys. Rev. A: At., Mol., Opt. Phys.* **2009**, *80*, 053826.
(47) Nayak, K. P.; Kien, F. L.; Kawai, Y.; Hakuta, K.; Nakajima, K.; Miyazaki, H. T.; Sugimoto, Y. Cavity formation on an optical nanofiber using focused ion beam milling technique. *Opt. Express* **2011**, *19*, 14040−14050.
(48) Henderson, M. R.; Gibson, B. C.; Ebendorff-Heidepriem, H.; Kuan, K.; Afshar V, S.; Orwa, J. O.; Aharonovich, I.; Tomljenovic-Hanic, S.; Greentree, A. D.; Prawer, S.; Monro, T. M. Diamond in Tellurite Glass: a New Medium for Quantum Information. *Adv. Mater. (Weinheim, Ger.)* **2011**, *23*, 2806−2810.
(49) Henderson, M. R.; Afshar V, S.; Greentree, A. D.; Monro, T. M. Dipole emitters in fiber: interface effects, collection efficiency and optimization. *Opt. Express* **2011**, *19*, 16182−16194.
(50) Yalla, R.; Le Kien, F.; Morinaga, M.; Hakuta, K. Efficient Channeling of Fluorescence Photons from Single Quantum Dots into Guided Modes of Optical Nanofiber. *Phys. Rev. Lett.* **2012**, *109*, 063602.
(51) Sumetsky, M. Nanophotonics of optical fibers. *Nanophotonics* **2013**, *2*, 393−406.
(52) Snyder, A. W.; Love, J. *Optical Waveguide Theory*, 1st ed.; Chapman and Hall Ltd, 1983.
(53) Jackson, J. D. *Classical Electrodynamics*, 3rd ed.; John Wiley & Sons, Inc., 1998.
(54) Grahn, P.; Shevchenko, A.; Kaivola, M. Electromagnetic multipole theory for optical nanomaterials. *New J. Phys.* **2012**, *14*, 093033.
(55) Tong, L.; Hu, L.; Zhang, J.; Qiu, J.; Yang, Q.; Lou, J.; Shen, Y.; He, J.; Z, Y. Photonic nanowires directly drawn from bulk glasses. *Opt. Express* **2006**, *14*, 82−87.
(56) Liao, M.; Gao, W.; Duan, Z.; Yan, X.; Suzuki, T.; Ohishi, Y. Directly draw highly nonlinear tellurite microstructured fiber with diameter varying sharply in a short fiber length. *Opt. Express* **2012**, *20*, 1141−1150.

DOI: 10.1021/acsphotonics.6b00030
ACS Photonics 2016, 3, 972−978